Ground Motion Prediction Equations for Arias Intensity, Cumulative Absolute Velocity, and Peak Incremental Ground Velocity for Rock Sites in Different Tectonic Environments

Zach Bullock[1], Shideh Dashti[2], Abbie Liel[3], Keith Porter[4], Zana Karimi[5], Brendon Bradley[6]

[1]Corresponding Author: PhD Student, Department of Civil, Environ. & Archit. Engrg, Univ. of Colorado Boulder, 1111 Engrg Dr. ECOT 441, Boulder, CO, 80309; e-mail: zachary.bullock@colorado.edu

[2]Assistant Professor, Department of Civil, Environ. & Archit. Engrg, Univ. of Colorado Boulder, 1111 Engrg Dr. ECOT 514, Boulder, CO, 80309; e-mail: shideh.dashti@colorado.edu

[3]Associate Professor, Department of Civil, Environ. & Archit. Engrg, Univ. of Colorado Boulder, 1111 Engrg Dr. ECOT 517, Boulder, CO, 80309; e-mail: abbie.liel@colorado.edu

[4]Research Professor, Department of Civil, Environ. & Archit. Engrg, Univ. of Colorado Boulder, 1111 Engrg Dr. ECOT 441, Boulder, CO, 80309; e-mail: keith.porter@colorado.edu

[5]Research Associate, Department of Civil, Environ. & Archit. Engrg, Univ. of Colorado Boulder, 1111 Engrg Dr. ECOT 441, Boulder, CO, 80309; e-mail: zana.karimi@colorado.edu

[6]Professor, Department of Civil & Nat. Res. Engrg., University of Canterbury, Private Bag 4800, Ilam, Christchurch, New Zealand, 8040; e-mail: brendon.bradley@canterbury.ac.nz

ABSTRACT

This paper presents the development of ground motion prediction equations (GMPEs) for the maximum rotated (RotD100) horizontal component of five intensity measures (IMs): Arias intensity (AI), cumulative absolute velocity (CAV), cumulative absolute velocity above the 5 cm/s^2 threshold (CAV_5), standardized cumulative absolute velocity (CAV_{STD}), and peak incremental ground velocity (V_{gi}). The equations predict the ground motion intensity at outcropping rock sites. This scope reflects the critical importance of outcropping rock motion properties that can be employed as predictors of certain site response quantities or used as input to site response and soil-structure interaction analyses. We present equations for the shallow crustal, intraplate, and subduction tectonic environments, and between- and within-event standard deviations for each. We also provide supplemental logistic models predicting the probability that CAV_5 and CAV_{STD} exceed zero in a given earthquake scenario. These equations are valid for magnitudes between 4.0 and 9.0 and source to site distances up to 400 km, depending on the tectonic environment.

BODY OF TEXT

INTRODUCTION

Kramer and Mitchell (2006) and Karimi and Dashti (2017a, 2017b) have shown that liquefaction hazard and its consequences (e.g., permanent foundation settlement) can be predicted more reliably through use of evolutionary intensity measures (IMs) rather than peak-transient measures (e.g., peak ground acceleration (PGA)). These measures are "evolutionary" because they accumulate over the course of a ground motion recording. They depend not only on the amplitude of motion, but also on the motion's duration and frequency content. One example of an evolutionary measure is cumulative absolute velocity. However, ground motion prediction equations for evolutionary intensity measures are fewer in number than those for traditional IMs such as peak spectral accelerations (PSA) and PGA. In addition, existing models for these evolutionary IMs have been developed using fewer ground motion records, and often apply to only one tectonic environment, generally shallow crustal active plate margins.

In this study, we propose new ground motion prediction equations for the maximum rotated (RotD100) horizontal component of Arias intensity (AI), cumulative absolute velocity (CAV), cumulative absolute velocity above a 5 cm/s^2 acceleration threshold (CAV_5), standardized cumulative absolute velocity (CAV_{STD}), and peak incremental ground velocity (V_{gi}). These equations predict these IMs as a function of earthquake (event) moment magnitude (M_w), focal depth (H), earthquake type and fault mechanism, and site distance to rupture (using closest distance, denoted R). We provide equations for shallow crustal, intraplate, and subduction tectonic environments. The resulting probabilistic estimates of these IMs provide inputs in the next stage of a performance-based framework for structural design or assessment, which would link these IMs to demand parameters (DPs) that relate to liquefaction-induced building

settlement or tilt. The primary motivation behind this work is to develop improved ground motion prediction equations for the evolutionary IMs that have been previously identified as the most efficient and sufficient predictors of liquefaction potential and consequences for structures. As a result, site effects (or terms) are not considered in the prediction equations in this study and we consider data only from rock sites ($V_{S,30}$ ranging from 600 to 2,100 m/s). For this specific and important problem, site effects are highly nonlinear and often require performing nonlinear site response analyses for the specific soil profile of interest. Furthermore, previous research by two of the authors (Karimi and Dashti 2017a, 2017b) showed that base rock motion properties (input excitation to the soil-structure system) tend to be good predictors of liquefaction induced building settlement and damage, in combination with the key properties of soil and structure. For these reasons, in this study, we focus on prediction equations for evolutionary IMs only on rock sites. These can be used for the liquefaction problem, or other cases where a soil model is combined with input (rock) excitation. The RotD100 component has been selected for use in this study because soil liquefaction and building settlement are expected to be correlated to the maximum intensity quantity, regardless of orientation. At sites where forward directivity is important, RotD100 aligns closely with the fault-normal component (Shahi and Baker 2014). Furthermore, Cubrinovski et al. (2003) showed that volumetric strains and excess pore pressure generation due to cyclic shearing are governed by the response in the direction of the maximum intensity of earthquake shaking.

REVIEW OF EXISTING PREDICTION EQUATIONS AND METHODOLOGIES

Douglas (2016) compiled a detailed summary of ground motion prediction equations (GMPEs) developed for PGA and PSA between 1964 and 2016. Recently, the NGA-West2 project (Bozorgnia et al. 2014) produced five empirical GMPEs for shallow crustal events using an

extensive, rich database of ground motion recordings. To develop the GMPEs, one of the NGA-West2 studies adopted a two-stage regression approach (Boore et al. 2014) while the others used a one-stage approach (Abrahamson et al. 2013; Campbell and Bozorgnia 2014; Chiou and Youngs 2014; Idriss 2014). Atkinson and Boore (2003), Abrahamson et al. (2016), and Morikawa and Fujiwara (2013) used the one-stage approach to develop empirical GMPEs for PGA and PSA in subduction earthquakes.

In the first stage of the two-stage approach (e.g., that of Boore et al. 2014), the path (distance-related) effects are isolated by subtracting the earthquake-by-earthquake average observation of PSA from all observations, and the dependence of these effects on distance is determined by regression. Within-event uncertainty is estimated in this stage. In the second stage, the dependence of the event effects on magnitude and mechanism is determined by regression and between-event uncertainty is estimated. In the one-stage approach utilized to develop the other GMPEs (e.g., Campbell and Bozorgnia 2014), weighted nonlinear regression is performed to determine all model coefficients at the same step. Joyner and Boore (1993) compared multistage (two-stage) and one-stage regression methodologies for analyzing strong motion data from earthquakes. Those authors conclude that both methods produce unbiased models and that the two-stage approach is marginally more computationally efficient. In all of the listed GMPEs, mixed-effects regression (which allows the separation of fixed and random effects) was used to estimate the uncertainty in model predictions. Mixed-effects regression is most often performed using the algorithm of Abrahamson and Youngs (1992) or the R implementation of Pinheiro et al. (2013).

When a ground motion database such as NGA-West is unavailable, a hybrid approach combining real ground motion recordings with stochastic simulations can be adopted. The most prominent

example of this methodology is the NGA-East project, which led to the development of synthetic ground motions for intraplate events (Boore 2015). These ground motions were employed in the development of hybrid GMPEs (Darragh et al. 2015; Pezeshk et al. 2015; Hollenback et al. 2015).

Fewer prediction equations exist for evolutionary intensity measures. However, research in both structural engineering and geotechnical engineering communities has highlighted the usefulness of these intensity measures in risk assessment (e.g., Harp and Wilson 1995; Kayen and Mitchell 1997; Benito and Herraiz 1997). A number of authors have developed broadly applicable models for AI based on shallow crustal records (Travasarou et al. 2003; Foulser-Piggott and Stafford 2012). Campbell and Bozorgnia (2010) published a model for AI and CAV, also considering shallow crustal records. Du and Wang (2013) developed a model for CAV based on shallow crustal records from the NGA database. Likewise, Kramer and Mitchell (2006) developed a model for CAV_5, and EPRI (2006) includes a model for CAV_{STD} based on records from the Western and Eastern United States. In addition, specialized prediction equations have been produced for AI in New Zealand (Stafford et al. 2009); AI in Japan (Pousse et al. 2006); AI in Italy (Sabetta and Pugliese 1996); AI and CAV in Japan (Foulser-Piggott and Goda 2015); and AI, CAV, and CAV_5 in Greece (Danciu and Tselentis 2007). All of these models used a one-stage regression approach. In addition, at least four prediction equations have been produced for significant duration: Kempton and Stewart (2006), Bommer et al. (2009), Bora et al. (2014); and Afshari and Stewart (2016). All four listed here used a one-stage regression approach and apply only in the shallow crustal tectonic environment.

Most of the models for evolutionary intensity measures have included terms for site effects. To capture these effects, the majority of records used in the development of these models are not

from rock sites, but rather from soil sites. The models developed in this study use exclusively records from rock sites to characterize attenuation and uncertainty for these sites only. The scope of these models reflects the motivation to predict the intensity of the base motion beneath the soil column. Further, no models for these IMs exist for the intraplate tectonic environment.

GROUND MOTION PREDICTION MODEL DEVELOPMENT

Ground Motion Record Collection

We collected ground motion records from sites with shear wave velocities in the top 30 m ($V_{S,30}$) exceeding 600 m/s, to represent rock conditions. This filter was applied to minimize the influence of softer rocks and soils on the motion properties. All selected records include metadata for the motions that includes magnitude and rupture distance from the sources described below. The complete shallow crustal database used in this study includes 2,191 records collected from the NGA-West database (Ancheta et al. 2012), 563 records collected from the New Zealand Strong Motion Database (Van Houtte et al. 2017, Kaiser et al. 2017), and 31 additional records from shallow strike-slip events in Alaska collected through COSMOS (Haddadi et al. 2008). The intraplate database consists of 1,098 records collected from the NGA-East database (Goulet et al. 2014). The subduction database consists of 1,252 records collected from the KiK/K-Net database. The subduction database contains only records from events that can be distinguished as subduction (interface) or subduction (in-slab) in the metadata collected by Foulser-Piggott and Goda (2015) and Dawood et al. (2016). These distinctions were developed on the basis of the source characteristics of each earthquake, its location, and, in the case of large events, detailed seismological studies of those individual events.

Additional records from the Internet Site for European Strong-Motion Data (ISESD) (Ambraseys et al. 2002) were considered for the crustal and intraplate databases, but the metadata for these

records was not as uniform as that for records from the NGA databases, so we excluded these records from the analysis. Additional records from subduction events in Chile, Northern California, and Washington were also considered, but these were all recorded at sites with soil or unknown conditions and were therefore excluded.

To exclude motions from low magnitude events recorded at sites far from the source, we applied linear magnitude-dependent distance filters to each database (e.g., R greater than 60 km for M_w 4.0 up to R greater than 200 km for M_w 5.5 for shallow crustal events; R greater than 100 km for M_w 4.0 up to R greater than 400 km for M_w 5.0 for intraplate events; and R greater than 150 km for M_w 4.0 up to R greater than 300 km for M_w 6.0 for subduction events). The removed records are unlikely to be of engineering significance. These filters resulted in 1,033 shallow crustal records, 141 intraplate records, and 1,237 subduction records being used in the final regression. Figure 1 shows the final distributions of event magnitude and site distance-to-rupture. Figure 2 reports the distributions of site shear wave velocity ($V_{S,30}$) for all records in each tectonic environment.

Intensity Measures Considered

The five intensity measures included in this study are: Arias intensity (AI), cumulative absolute velocity (CAV), cumulative absolute velocity above a 5 cm/s^2 acceleration threshold (CAV_5), standardized cumulative absolute velocity (CAV_{STD}), and peak incremental ground velocity (V_{gi}). Table 1 defines these IMs.

In the equation for CAV_5 presented in Table 1, χ is a filter that has a value of 1 if the acceleration at that time step exceeds 5 cm/s^2 or a value of 0 if it does not, i.e., the Heaviside step function $\chi = H(a - 5\ cm/sec^2)$. In the equation for CAV_{STD}, each non-overlapping one-second time increment is considered separately in the summation, N is the total number of such increments of time, and

179 PGA_i is the peak ground acceleration in the *i*-th increment. In the equation for V_{gi}, t_1^i and t_2^i are
180 the times marking the beginning and end of the *i*-th acceleration pulse. The integrals for AI,
181 CAV, and CAV_5 are from time zero to the duration of the record.

182 Each intensity measure is evolutionary in nature and is influenced by the amplitude, frequency
183 content, and duration of the ground motion. Figure 3 and Figure 4 show the trends in intensity
184 (as represented by CAV) with respect to magnitude and site to source distance, respectively, for
185 all three tectonic environments considered. For brevity, all figures in this study will show CAV,
186 although the trends in the other IMs are similar.

187 Among the IMs considered, AI and CAV are the most commonly used and are the subject of a
188 greater number of previous GMPEs. As shown in Table 1, AI and CAV are defined as the
189 integral of the record acceleration squared and the integral of the absolute value of the record
190 acceleration, respectively. Due to this mathematical difference in their definition, AI naturally
191 exhibits a broader scatter than CAV and is more sensitive to high frequency ground motion
192 content. This has been reflected in the logarithmic standard deviations of previous ground motion
193 prediction equations that have considered both intensity measures using identical databases (e.g.,
194 Danciu and Tselentis 2007; Campbell and Bozorgnia 2010; and Foulser-Piggott and Goda 2015).

195 Previous research has shown CAV_5 to be a strong predictor of both liquefaction triggering and
196 resulting settlements under shallow-founded structures (Kramer and Mitchell 2006; Karimi and
197 Dashti 2017b). Kramer and Mitchell (2006) demonstrated the predictability of CAV_5 by a
198 GMPE, but CAV_5 is inherently more difficult to predict than CAV due to the zero value it takes
199 on below the acceleration threshold. Here, we use "predictability" to mean that it is possible to
200 construct a regression model that predicts a given IM with reasonable goodness-of-fit and
201 acceptable uncertainty as reflected in the standard deviation of residuals. Predictability is an

important characteristic of GMPEs because uncertainty in these equations is carried into each subsequent phase of a performance-based procedure or probabilistic hazard analysis.

In order for CAV_5 and CAV_{STD} to take on a nonzero value, the RotD100 value of PGA must exceed 5 cm/s^2 or 0.025*g*, respectively. This threshold reduces the number of records available to model these IMs. Additionally, the transformation from CAV to CAV_5 or CAV_{STD} affects each record in a somewhat arbitrary way, which may contribute to increased scatter in CAV_5 and CAV_{STD}. In addition to increasing model uncertainty in these two ways, these limitations have the effect of creating bias towards stronger motions since weaker motions are systematically excluded. In this study, because the predictions of these regression models for CAV_5 and CAV_{STD} are necessarily conditioned on the given IM taking on a nonzero value, logistic regression (Cox 1958) was developed following a similar procedure to Bray and Travasarou (2007), which applied a probit regression approach to account for zero-valued slope displacements.

In addition to being more novel and less-researched, the peak incremental ground velocity (V_{gi}) is different from the other four intensity measures considered in this paper in that it does not depend on the total duration of the record, but rather only on the intensity and duration of the largest acceleration pulse. We defined acceleration pulses as portions of the ground motion records starting at a zero crossing and including two additional zero crossings, or essentially one cycle in the acceleration time history. The V_{gi} of a given record is the largest area under any single pulse in that record. V_{gi} has been shown to be useful in applications related to design and assessment of frictional base isolators (Jampole et al. 2016), where it correlates strongly with the largest excursion of the isolator. It may also have applications in geotechnical earthquake engineering.

Regression Methodology

We considered multistage and one-stage mixed-effects regression methodologies, but each yielded similar results. We therefore adopted a single-stage mixed effects regression approach using the methodology of Abrahamson and Youngs (1992), consistent with many of the aforementioned prediction equations. A reader interested in the details of each step of the regression is therefore referred to Abrahamson and Youngs (1992).

Equation 1 provides the general form of regression using this methodology.

$$ln\, Y_{i,j} = f\left(M_i, R_{i,j}, \dots\right) + \eta_i + \varepsilon_{i,j} \qquad (1)$$

In Equation 1, the subscript *i* refers to parameters of the *i*-th event and the subscript *j* refers to parameters of the *j*-th recording from that event. The terms in the functional form $f\,(M_i, R_{i,j}, \dots)$ are treated as fixed effects, while the between-event logarithmic residual for the *i*-th event, η_i, and the within-event logarithmic residual for the *j*-th recording in the *i*-th event, $\varepsilon_{i,j}$, are treated as random effects. We assumed the between- and within-event logarithmic residuals to be normally distributed with zero mean and standard deviations equal to the between- and within-event standard deviations (τ and ϕ), respectively. The total logarithmic residual, $r_{i,j}$, is the sum of η_i and $\varepsilon_{i,j}$. This treatment of mixed-effects regression follows the methodology of many previous GMPEs (e.g., Boore et al. 2013, Abrahamson et al. 2013, and Campbell and Bozorgnia 2013).

We neglected site effects because all records considered were recorded on rock. Although the database includes rock outcrops with different $V_{S,30}$ values, we assumed that there is no statistical difference between these IMs measured on weathered rock or intact rock. We validated this

assumption post facto by evaluating the residuals as a function of rock shear wave velocity ($V_{S,30}$).

Functional Form Selection

Development of the functional form for this study began by considering the form used by Travasarou et al. (2003) for AI and, later by Kramer and Mitchell (2006) for CAV_5:

$$ln\,Y = c_1 + c_2(M_W - 6) + c_3\,ln(M_W/6) + c_4\,ln\left(\sqrt{R^2 + h^2}\right) + f_1F_N + f_2F_R \qquad (2)$$

In Equation 2, M_W is the moment magnitude, R is the distance to rupture in kilometers, F_N is a flag for faulting mechanism that is equal to 1 if the faulting mechanism is normal and 0 otherwise, and F_R is a flag for faulting mechanism that is equal to 1 if the faulting mechanism is reverse and 0 otherwise. This form is appealing because it has been previously shown to be effective in predicting IMs like those considered and because it is well-constrained at close distances due to the fictitious depth term, *h*. However, this form was found to be unable to adequately capture the trends found in the datasets used in this study as judged by the resulting R^2 statistic of the model and the standard deviation of its residuals.

In a second attempt, because the IMs considered are fundamentally tied to the duration of the ground motion, the form used by Kempton and Stewart (2006) to predict significant duration was also considered:

$$ln\,SD = ln\left[\frac{\left(\frac{\Delta\sigma}{10^{1.5M_W+16.05}}\right)^{-\frac{1}{3}}}{4.9\cdot10^6\beta} + c_2R + f_2(S)\right] \qquad (3)$$

Ultimately, a new form incorporating elements of both of the above forms was adopted. The final functional form used in this study for the shallow crustal and intraplate tectonic environments was:

$$ln\,\bar{Y} = a_0 + a_1 M_W + a_2 M_W^2 + (b_1 + b_2 M_W)\,ln\,R + b_3 R + f_1 F_R + f_2 F_N \qquad (4)$$

We report all model coefficients in Table 2. The predictions made using these coefficients are all in units of centimeters and seconds. This functional form includes: quadratic scaling of intensity with magnitude, found in many GMPEs for PGA and PSA (e.g., Boore et al. 2014, Idriss 2014); magnitude-dependent log-linear scaling with distance, similar to that employed by Campbell and Bozorgnia (2014) for PGA and PSA, Travasarou et al. (2003) for AI, and Bommer et al. (2009) for significant duration; linear scaling with distance, as seen in Kempton and Stewart (2006) for significant duration; and dependence on mechanism type, which is ubiquitous in GMPEs, especially those developed for the shallow crustal tectonic environment.

For the subduction tectonic environment, the geometric attenuation is more complex. For this case, we considered the functional forms used by Atkinson and Boore (2003) for PSA and Foulser-Piggott and Goda (2015) for AI and CAV for subduction earthquakes. The final functional form adopted for the subduction tectonic environments was:

$$ln\,\bar{Y} = a_0 + a_1 M_W + a_2 M_W^2 + (b_1 + b_2 M_W)\,ln\,D + b_3 D + b_4 H \qquad (5)$$

Two sets of model coefficients were developed to capture the difference in the trends observed in interface and in-slab events. We also provide coefficients for use when this information is unknown. Here, M_W is the moment magnitude, R is the distance to rupture in kilometers, and H is the focal depth in kilometers. In the functional form for subduction, D is a distance that has been modified with a magnitude-dependent near-source saturation term, Δ, which is given by:

$$D = \sqrt{R^2 + \Delta^2} \quad (6)$$

$$\Delta = 0.00724 \times 10^{0.507 \times min(M_W, 8)} \quad (7)$$

Atkinson and Boore (2003) derived this magnitude-dependent near-source saturation term. As in that study, we considered other definitions of Δ. Determining Δ by regression, both as a constant and as a function of magnitude with the same form, did not improve model performance. Adjusting the maximum considered magnitude between 7.5 and 9.0 had an adverse effect on model performance in terms of the model R^2 statistic and the standard deviation of the model residuals, and considering different maximum magnitudes for interface and in-slab events had little impact. Due to the neutral or adverse effect of changing this magnitude threshold, we recommend simply using 8.0 for both event types, as shown in Equation7. Intraslab earthquakes generally occur at great depths, and the resulting lack of near-source recordings for intraslab events makes it difficult to identify near-source saturation in these earthquakes. However, including this term as opposed to unadjusted distance terms improved model performance for intraslab events as represented by the model R^2 statistic, as well as for interface events, so it was used for subduction events of all types. Atkinson and Boore (2003) previously used this term for developing a GMPE using a database that included both interface and intraslab events.

We considered an assortment of other terms used in previous GMPEs for each tectonic environment, including hinge magnitudes, additional distance measures (such as R_{JB} and R_x), hanging wall terms, fictitious depth terms, a term for depth-to-top of rupture (Z_{TOR}), site terms, and regional adjustments. However, the terms investigated did not appear to improve the model predictions, as measured in terms of the model R^2 statistic, the standard deviation of the model

307 residuals, and the statistical significance of these individual terms as reflected in their *p*-values.
308 We therefore did not include these terms in the functional form.

309 Table 2 provides the model coefficients for all intensity measures investigated in this paper and
310 all tectonic environments. Figure 5 and Figure 6 plot the shape of the models' attenuation for
311 CAV for the shallow crustal and subduction tectonic environments, respectively. The proposed
312 models' shape is compared with other models in the literature and actual recordings from
313 previous earthquakes as validation, as discussed later in the paper. No previous models for the
314 IMs considered in this study exist for the intraplate tectonic environment, but the shape of the
315 attenuation found in this study is shown in Figure 7. There are too few records available to
316 develop a model for CAV_{STD} in the intraplate tectonic environment, so this IM was excluded.
317 Plots similar to Figures 5 through 7 for other IMs are included in the electronic supplement.

318 **Logistic Regression for CAV_5 and CAV_{STD}**

319 As previously described, predictions of CAV_5 and CAV_{STD} made using the presented model are
320 necessarily conditioned on these IMs taking on nonzero values. Therefore, the probability of
321 either IM exceeding a given value can be determined by:

322 $$P(y > Y) = P(y > Y|y > 0)P(y > 0) \quad (8)$$

323 The term $P(y > Y|y > 0)$ is obtained from the models in Table 2 based on the predicted median
324 $\ln \bar{Y}$. To quantify $P(y > 0)$, we performed logistic regression to determine the probability of
325 each of these IMs exceeding zero as a function of magnitude, distance, and focal depth. The
326 functional form of the logistic regression is:

327 $$P(y > 0) = \left(\frac{exp(z)}{1+exp(z)}\right) \quad (9)$$

$$z = \alpha_0 + \alpha_1 M_W + \beta_1 \ln R + \beta_2 R + \beta_3 H \quad (10)$$

Initially, we used the same functional form used for the regression models in place of Equation 10, but several terms had little effect on the predicted probabilities, and were therefore removed. The formulation in Equation 9 is typical for estimating probabilities by logistic regression, per its original presentation (Cox 1958). Equation 9 can be very closely estimated by using the normal CDF according to Equation 11. Note that we provide Equation 11 on the basis of empirical approximation.

$$P(y > 0) \cong \Phi(z/1.695) \quad (11)$$

Table 3 provides the coefficients for this model. Figure 8 illustrates the resulting probabilities for CAV_5. Performing this analysis for interface and intraslab subduction events separately generated similar results, so we provide a single logistic model developed using the entire database of subduction motions. For ranges of magnitude and distance that are of engineering significance, these probabilities approach 1.

Alternatively, any ground motion prediction equation for PGA can be applied to approximate the probability that either of these IMs exceeds zero. To determine this probability using a GMPE, the following equation can be applied:

$$P(y > 0) = 1 - \Phi\left(\frac{\ln X - \ln \bar{Y}}{\sigma_T}\right) \quad (12)$$

In this equation, $\bar{Y}$ is the median PGA predicted by a given GMPE for a given scenario, σ_T is the total logarithmic standard deviation provided by a given GMPE, and X is 5 cm/s^2 or 0.025g for CAV_5 and CAV_{STD}, respectively. This is an approximation because it is based on the probability that the PGA as defined in the GMPE exceeds that threshold. This PGA may be the geometric mean of the two horizontal components, the PGA of the median rotated ground motion

(RotD50), or another measure of PGA, depending on the GMPE used. The logistic regression method developed previously is based on the probability that the RotD100 PGA exceeds the threshold, which is consistent with the limitations on the data in the regression models above.

MODEL EVALUATION

Residual Analysis

We analyzed the model residuals to identify bias and estimate the uncertainty in the model predictions. Figure 9, Figure 10, and Figure 11 show the total logarithmic residuals of the model predictions of CAV for the shallow crustal, intraplate, and subduction tectonic environments, respectively. The moving averages shown use a 50-point window for shallow crustal (approximately 5% of the population), a 10-point window for intraplate (14%), and a 50-point window for subduction (4%). There is no evident bias in the model for any of the predictor variables shown, including those that were excluded in the final functional forms, such as the depth-to-top of rupture (Z_{TOR}) and the centroidal depth (Z_{CMT}). The centroidal depth, as available in the NGA East database metadata, is defined as the depth to the centroid of the finite rupture model for a given earthquake. These measures are included in this figure despite being excluded from the functional form to demonstrate that there is no apparent advantage of considering these terms. The residuals of each model pass a Lilliefors normality test for all intensity measures considered.

Figure 12, Figure 13, and Figure 14 show the between- and within-event residuals for the shallow crustal, intraplate, and subduction tectonic environments, respectively. There is likewise no evident bias in the model for any of the predictor variables for the decomposed residuals. In particular, the lack of bias with respect to site shear wave velocity validates the assumption that

site effects have been excluded by selecting only records from rock sites. The electronic supplement provides plots similar to Figures 9 through 14 for the other IMs.

Estimated Model Uncertainty

We assumed all model standard deviations to be homoscedastic, with values reported in Table 2. Figure 15 compares the final model values with the smoothed empirical between- and within-event standard deviations for CAV for each tectonic environment. In general, the between- and within-event standard deviations do not display any clear heteroscedasticity, supporting the assumption of homoscedasticity. In the case of the subduction model, the data set is sparser above magnitude 7.5 than in the range between 5.5 and 7.5 (Figure 3), likely accounting for the sharp decrease in the between-event standard deviations observed above a magnitude of 7.5. Rather than fitting a model where this between-event standard deviation drops above magnitude 7.5, we selected the model value for this case to avoid underestimating the uncertainty. The uncertainty for the subduction model was determined using the entire set of subduction motions and is the same for intraslab and interface events. Estimating this uncertainty separately for each type of subduction event resulted in similar results for both.

Comparison with Existing Models

Table 4 compares the models developed in this study and a variety of existing models in terms of applicability, size of database, and total logarithmic standard deviation for shallow crustal and subduction events. No model for any of the IMs considered is available for intraplate events.

In reporting this comparison, when the number of rock records used in a study or its range of applicability was not explicitly reported, we estimated these numbers based on figures in the paper. For the Foulser-Piggott and Goda (2015), we could not ascertain the number of rock

394 records included because the subduction records and shallow crustal records are shown in the
395 same figure. Kramer and Mitchell (2006) targeted a site shear wave velocity of 760 m/s rather
396 than including records from rock sites of varying quality. Danciu and Tselentis (2007) used only
397 records from Greece; Stafford et al. (2009) predicted AI specifically for New Zealand.

398 In all cases, our database includes more rock records than previous studies. The range of
399 applicability of the model is comparable or wider for moment magnitude for all IMs in both of
400 the tectonic environments included in the comparison, and generally comparable or larger for
401 distance to rupture, with the exception of the wider ranges of Travasarou et al. (2003) and
402 Stafford et al. (2009) for AI in the shallow crustal environment. The total logarithmic standard
403 deviations for this model in the shallow crustal tectonic environment fall in the range observed in
404 other models for AI, but are slightly larger for CAV and CAV_5 in that environment. The total
405 logarithmic standard deviations for this model in the subduction environment are smaller than
406 those reported for other models.

407 It is noteworthy that the between-event standard deviations in this study are larger than in other
408 studies for the same IMs. The values derived here for CAV are approximately 0.40 for shallow
409 crustal events in this study, whereas those of Campbell and Bozorgnia (2010) are approximately
410 0.2. They are also large when compared internally with the within-event standard deviations
411 (approximately 0.33 for shallow crustal events). Commonly, within-event standard-deviations
412 are larger than the between-event (Shahi and Baker 2014).

413 Why might our between-event residual standard deviation of 0.40 be larger than that of prior
414 authors? Perhaps our exclusive use of rock records produces greater correlation of wave
415 velocities at different points along the path of wave propagation. With more-uniform wave
416 velocity, waves will tend to retain coherence for more wavelengths. Because the path is generally

417 through rock, with generally higher wave velocity and larger wavelength, the more-coherent
418 waves will also tend to reach the surface in fewer wavelengths, increasing the effect of
419 coherence. We think one can characterize that coherence as positive correlation in wave velocity
420 and amplitude at different points along the path and between different paths from the rupture
421 surface to the ground surface.
422 We do not believe that these two effects – fewer wavelengths to travel the same distance and
423 greater coherence in the same number of wavelengths – would reduce variability in ground
424 motion at the surface, but instead suspect would increase variance. Why? There remains inherent
425 uncertainty in the amplitude of seismic waves leaving a rupture of a given magnitude. Motion at
426 the ground surface where they arrive represents a sum of random variables: the uncertain values
427 of wave amplitude from waves traveling along different paths from the rupture surface and
428 arriving at the same place at the same time. In general, the sum of correlated random variables
429 has variance that is larger than the sum of their individual variances, larger by an amount that
430 increases with their covariances. So by limiting records to rock sites only, perhaps one could
431 rather expect greater variance in the ground motion at the surface than one would observe with
432 mixed sites. We offer the foregoing merely as a plausible hypothesis, one requiring further study
433 to test how well it reflects reality.
434 We compared the models developed in this study to those of Campbell and Bozorgnia (2010) for
435 CAV in shallow crustal events and Foulser-Piggott and Goda (2015) for CAV in subduction
436 events in Figure 5 and Figure 6, respectively. We chose to compare our model for shallow crustal
437 events to that of Campbell and Bozorgnia (2010) rather than that of Du and Wang (2013)
438 because the latter acknowledges bias for $V_{S,30}$ values in the range of most interest for our model.
439 These figures show the medians plus and minus one standard deviation for the models being

compared, as well as the rock records in the database from the selected earthquakes. In both cases, the model developed in this study provides a better fit through the rock records from the given events. Additionally, the model developed in this study for the subduction tectonic environment appears to be better constrained at near distances due to the inclusion of the near-source saturation term.

CONCLUDING REMARKS

We developed ground motion prediction equations for the RotD100 horizontal component of Arias intensity (AI), cumulative absolute velocity (CAV), cumulative absolute velocity above a 5 cm/s^2 threshold (CAV_5), standardized cumulative velocity (CAV_{STD}), and peak incremental ground velocity (V_{gi}). The models are applicable for shallow crustal events of moment magnitudes between 4 and 8 at distances up to 200 km, for intraplate events of magnitudes between 4 and 6 at distances up to 400 km, and for subduction events of magnitudes between 4 and 9 at distances up to 300 km and focal depths up to 180 km. We provide supplemental logistic models to calculate the probability that CAV_5 and CAV_{STD} exceed zero in a given earthquake scenario for all three tectonic environments.

The models can be used to predict the motion at outcropping rock sites and are intended for use as input to site response and soil-structure interaction analyses and for applications where the base rock motion is better suited for use as the predictor of certain demand parameters, such as liquefaction-induced settlement. We have shown the models to be unbiased on their predictor variables as well as additional source and site characteristics that were excluded from the functional form. In particular, site shear wave velocity is not included in the functional form of this study.

462 For the specific case of predicting ground motion intensity on outcropping rock sites, the models
463 in this study are based on more robust databases than used in previous models. The quality of the
464 fit of these models to records from rock sites has also been shown to improve on that of other
465 models which include site effects. In the case of the model for the subduction tectonic
466 environment, the functional form used in this study is better constrained at low distances than
467 previous models. Previous models did not include the intraplate tectonic environment. For these
468 reasons, the models presented here are better suited for use in cases that require prediction of
469 motion on outcropping rock and are more broadly applicable in terms of tectonic environment.

DATA AND RESOURCES

The following databases were used to gather data for this study and can be accessed at the following URLs: the NGA-West Database (http://ngawest2.berkeley.edu/); the NGA-East Database (http://ngawest2.berkeley.edu/); the Kiban-Kyoshin network (http://www.kyoshin.bosai.go.jp/); the New Zealand Strong Motion Database (http://info.geonet.org.nz/display/appdata/The+New+Zealand+Strong-Motion+Database); the Internet Site for the European Strong-Motion Database (http://www.isesd.hi.is/); and the Center for Engineering Strong Motion Data database (http://strongmotioncenter.org/vdc/scripts/search.plx). Each of these databases was last accessed on 18 December, 2016. The electronic supplement provides lists of the records used in this study.

Additionally, the authors referred to a compilation of ground motion prediction equations provided by Douglas online (Douglas, J. (2016). *Ground-motion prediction equations 1964-2016*, http://www.gmpe.org.uk). This website was also last accessed 18 December, 2016.

ACKNOWLEDGEMENTS

Support for this research was provided partly by the Department of Education under award number P200A150042 and partly by the Department of Civil, Environmental, and Architectural Engineering at the University of Colorado Boulder. Any opinions, findings, and conclusions or recommendations expressed in this material are those of the authors and do not necessarily reflect the views of the Department of Education. The authors would like to acknowledge Professor Katsuichiro Goda of the University of Bristol for providing his classifications of subduction events in the KiK/K-Net database and his assistance with implementing the Foulser-Piggott and Goda (2015) model.

REFERENCES

Abrahamson, N. A., & Youngs, R. R. (1992). A stable algorithm for regression analyses using the random effects model. *Bulletin of the Seismological Society of America, 82*(1), 505-510.

Abrahamson, N. A., Silva, W. J., & Kamai, R. (2013). Update of the AS08 Ground-Motion Prediction equations based on the NGA-west2 data set. *Pacific Earthquake Engineering Research Center Report, 2013/04.*

Abrahamson, N., Gregor, N., & Addo, K. (2016). BC Hydro ground motion prediction equations for subduction earthquakes. *Earthquake Spectra, 32*(1), 23-44.

Afshari, K., & Stewart, J. P. (2016). Physically Parameterized Prediction Equations for Significant Duration in Active Crustal Regions. *Earthquake Spectra,* In Press.

Ambraseys, N., Smit, P., Sigbjornsson, R., Suhadolc, P. and Margaris, B. (2002), Internet-Site for European Strong-Motion Data, *European Commission, Research-Directorate General, Environment and Climate Programme*.

Ancheta, T. D., Darragh, R. B., Stewart, J. P., Seyhan, E., Silva, W. J., Chiou, B. S. J., Woodell, K. E., Graves, R. W., Kottke, A. R., Boore, D. M., Kishida, T., & Donahue, J. L. (2014). NGA-West2 database. *Earthquake Spectra, 30*(3), 989-1005.

Arias, A. (1970). A measure of earthquake intensity. In R. J. Hansen (Ed.), *Seismic Design for Nuclear Power Plants.* (pp 438-483). Cambridge, MA: MIT Press.

Atkinson, G. M., & Boore, D. M. (2003). Empirical ground-motion relations for subduction-zone earthquakes and their application to Cascadia and other regions. *Bulletin of the Seismological Society of America, 93*(4), 1703-1729.

Benito, B., & Herraiz, M. (1997). An approach to the measurement of the potential structural damage of earthquake ground motions. *Earthquake Engineering and Structural Dynamics, 26,* 79-92.

Boore, D. (2015). Point-Source Stochastic Method Simulations of Ground Motions for the PEER NGA-East Project. *Pacific Earthquake Engineering Research Center Report 2015/04.*

Boore, D. M., Stewart, J. P., Seyhan, E., & Atkinson, G. M. (2014). NGA-West2 equations for predicting PGA, PGV, and 5% damped PSA for shallow crustal earthquakes. *Earthquake Spectra*, *30*(3), 1057-1085.

Bommer, J. J., Stafford, P. J., & Alarcón, J. E. (2009). Empirical equations for the prediction of the significant, bracketed, and uniform duration of earthquake ground motion. *Bulletin of the Seismological Society of America*, *99*(6), 3217-3233.

Bora, S. S., Scherbaum, F., Kuehn, N., & Stafford, P. (2014). Fourier spectral-and duration models for the generation of response spectra adjustable to different source-, propagation-, and site conditions. *Bulletin of Earthquake Engineering*, *12*(1), 467-493.

Bozorgnia, Y., Abrahamson, N. A., Atik, L. A., Ancheta, T. D., Atkinson, G. M., Baker, J. W., Baltay, A., Boore D. M., Campbell, K. W., Chiou, B. S. J., Darragh, R., Day, S., Donahue, J., Graves, R. W., Gregor, N., Hanks, T., Idriss, I. M., Kamai, R., Kishida, T., Kottke, A., Mahin, S. A., Rezaeian, S., Rowshandel, B., Seyhan, E., Shahi, S., Shantz, T., Silva, W., Spudich, P., Stewart, J. P., Watson-Lamprey, J., Woodell, K., & Youngs, R. (2014). NGA-West2 research project. *Earthquake Spectra*, *30*(3), 973-987.

Bray, J. D., & Travasarou, T. (2007). Simplified procedure for estimating earthquake-induced deviatoric slope displacements. *Journal of Geotechnical and Geoenvironmental Engineering*, *133*(4), 381-392.

Campbell, K. W., & Bozorgnia, Y. (2012). A comparison of ground motion prediction equations for Arias intensity and cumulative absolute velocity developed using a consistent database and functional form. *Earthquake Spectra*, *28*(3), 931-941.

538 Campbell, K. W., & Bozorgnia, Y. (2014). NGA-West2 ground motion model for the average horizontal
539 components of PGA, PGV, and 5% damped linear acceleration response spectra. *Earthquake*
540 *Spectra*, *30*(3), 1087-1115.
541 Chiou, B. S. J., & Youngs, R. R. (2014). Update of the Chiou and Youngs NGA model for the average
542 horizontal component of peak ground motion and response spectra. *Earthquake Spectra*, *30*(3), 1117-
543 1153.
544 Cox, D. R. (1958). The regression analysis of binary sequences. *Journal of the Royal Statistical*
545 *Society. Series B (Methodological)*, 215-242.

546 Cubrinovski, M., Ishihara, K., & Shibayama, T. (2003). Seismic 3-D effective stress analysis:
547 constitutive modelling and application. In *Proc. 3rd Int. Conf. Deformation Characteristics of*
548 *Geomaterials*.

549 Danciu, L., & Tselentis, G. A. (2007). Engineering ground-motion parameters attenuation
550 relationships for Greece. *Bulletin of the Seismological Society of America*, *97*(1B), 162-183.

551 Darragh, R. B., Abrahamson, N. A., Silva, W. J., & Gregor, N. (2015). NGA-East: Median Ground-
552 Motion Models for the Central and Eastern North America Region. *Pacific Earthquake Engineering*
553 *Research Center Report 2015/04.*

554 Dawood, H. M., Rodriguez-Marek, A., Bayless, J., Goulet, C., & Thompson, E. (2016). A Flatfile for the
555 KiK-net Database Processed Using an Automated Protocol. *Earthquake Spectra*, *32*(2), 1281-1302.

556 Du, W., & Wang, G. (2013). A Simple Ground-motion Prediction Model for Cumulative Absolute
557 Velocity and Model Validation. *Earthquake Engineering & Structural Dynamics*, *42*(8), 1189-1202.

558 Electric Power Research Institute. (1988). A Criterion for Determining Exceedances of the Operating
559 Basis Earthquake, EPRI Report NP-5930. *Electric Power Research Institute, Palo Alto*.

560 Electric Power Research Institute. (2006). Program on technology innovation: Use of cumulative absolute
561 velocity (CAV) in determining effects of small magnitude earthquakes on seismic hazard analyses. *EPRI,*
562 *Palo Alto, CA, and the US Department of Energy, Germantown. EPRI report MD, 1014099*.Foulser-
563 Piggott, R., & Goda, K. (2015). Ground-Motion Prediction Models for Arias Intensity and Cumulative
564 Absolute Velocity for Japanese Earthquakes Considering Single-Station Sigma and Within-Event Spatial
565 Correlation. *Bulletin of the Seismological Society of America*, *105*(4), 1903-1918.

566 Foulser-Piggott, R., & Stafford, P. J. (2012). A predictive model for Arias intensity at multiple sites and
567 consideration of spatial correlations. *Earthquake Engineering & Structural Dynamics*, *41*(3), 431-451.

568 Goulet, C. A., Kishida, T., Ancheta, T., Cramer, C. H., Darragh, R. B., Silva, W. J., Hashash, Y. M. A.,
569 Harmon, J., Stewart, J. P., Woodell, K. E., & Youngs, R. R. (2014). PEER NGA-East database. *Pacific*
570 *Earthquake Engineering Research Center Report 2014/17*.

571 Haddadi, H., Shakal, A., Stephens, C., Savage, W., Huang, M., Leith, W., & Parrish, J. (2008). Center for
572 Engineering Strong-Motion Data (CESMD). In *Proceedings of the 14th World Conference on Earthquake*
573 *Engineering*. Beijing, China.

574 Harp, E. L., & Wilson, R. C. (1995). Shaking intensity thresholds for rock falls and slides: Evidence from
575 1987 Whittier Narrows and superstition hills earthquake strong-motion records. *Bulletin of the*
576 *Seismological Society of America*, *85*(6), 1739-1757.

577 Hollenback, J., Kuehn, N., Goulet, C., & Abrahamson, N.A. (2015). PEER NGA-East Median Ground-
578 Motion Models. *Pacific Earthquake Engineering Research Center Report 2015/04.*

579 Idriss, I. M. (2014). An NGA-West2 empirical model for estimating the horizontal spectral values
580 generated by shallow crustal earthquakes. *Earthquake Spectra*, *30*(3), 1155-1177.

581 Jampole, E., Deierlein, G., Miranda, E., Fell, B., Swensen, S., & Acevedo, C. (2016). Full scale dynamic
582 testing of a sliding seismically isolated unibody house. *Earthquake Spectra*, In Press.

583 Joyner, W. B., & Boore, D. M. (1993). Methods for regression analysis of strong-motion data. *Bulletin of*
584 *the Seismological Society of America*, *83*(2), 469-487.

585 Kaiser, A., Van Houtte, C., Perrin, N., Wotherspoon, L., McVerry, G. (2017). Site characterisation
586 of GeoNet stations for the New Zealand strong motion database. *Bulletin of the New Zealand Society*
587 *for Earthquake Engineering*, In Press.

588 Karimi, Z., & Dashti, S. (2017). Ground motion intensity measures to evaluate I: the liquefaction hazard
589 in the vicinity of shallow-founded structures. *Earthquake Spectra*, In Press.

590 Karimi, Z. & Dashti, S. (2017) Ground motion intensity measures to evaluate II: the performance of
591 shallow-founded structures on liquefiable ground. *Earthquake Spectra*, In Press.

592 Kayen, R. E., & Mitchell, J. K. (1997). Assessment of liquefaction potential during earthquakes by Arias
593 intensity. *Journal of Geotechnical and Geoenvironmental Engineering*, *123*(12), 1162-1174.

594 Kempton, J. J., & Stewart, J. P. (2006). Prediction equations for significant duration of earthquake ground
595 motions considering site and near-source effects. *Earthquake Spectra*, *22*(4), 985-1013.

596 Kramer, S. L., & Mitchell, R. A. (2006). Ground motion intensity measures for liquefaction hazard
597 evaluation. *Earthquake Spectra*, *22*(2), 413-438.

598 Morikawa, N., & Fujiwara, H. (2013). A new ground motion prediction equation for Japan applicable up
599 to M9 mega-earthquake. *Journal of Disaster Research*, *8*(5), 878-888.

600 Pezeshk, S., Zandieh, A., Campbell, K. W., & Tavakoli, B. (2015). Ground motion prediction equations
601 for eastern North America using the hybrid empirical method and NGA-West2 empirical ground motion
602 model. *NGA-East: Median Ground Motion Models for the Central and Eastern North America Region*,
603 119-147.

Pinheiro, H., Bates, D., DebRoy, S., Sarkar, D., and the R Development Core Team, 2013. NLME: Linear and Nonlinear Mixed Effects Models, R package version 3.1–108.

Pousse, G., Bonilla, L. F., Cotton, F., & Margerin, L. (2006). Nonstationary stochastic simulation of strong ground motion time histories including natural variability: Application to the K-net Japanese database. *Bulletin of the Seismological Society of America*, *96*(6), 2103-2117.

Sabetta, F., & Pugliese, A. (1996). Estimation of response spectra and simulation of nonstationary earthquake ground motions. *Bulletin of the Seismological Society of America*, *86*(2), 337-352.

Shahi, S. K., & Baker, J. W. (2014). NGA-West2 Models for Ground Motion Directionality. *Earthquake Spectra*, *30*(3), 1285-1300.

Stafford, P. J., Berrill, J. B., & Pettinga, J. R. (2009). New predictive equations for Arias intensity from crustal earthquakes in New Zealand. *Journal of Seismology*, *13*(1), 31-52.

Travasarou, T., Bray, J. D., & Abrahamson, N. A. (2003). Empirical attenuation relationship for Arias intensity. *Earthquake Engineering & Structural Dynamics*, *32*(7), 1133-1155.

Van Houtte, C., Bannister, S., Holden, C., Bourguignon, S., McVerry, G. (2017). The New Zealand Strong Motion Database. *Bulletin of the New Zealand Society for Earthquake Engineering*, In press.

MAILING ADDRESSES OF EACH AUTHOR

Zach Bullock:

1111 Engineering Drive
ECOT 441
Boulder, CO, 80309

Shideh Dashti:

1111 Engineering Drive
ECOT 514
Boulder, CO, 80309

Abbie Liel:

1111 Engineering Drive
ECOT 517
Boulder, CO, 80309

Keith Porter:

1111 Engineering Drive
ECOT 441
Boulder, CO, 80309

Zana Karimi:

1111 Engineering Drive
ECOT 441
Boulder, CO, 80309

Brendon Bradley:

Private Bag 4800
Ilam, Christchurch
New Zealand, 8040

TABLE CAPTIONS

Table 1: Definitions of the considered intensity measures

Table 2: Regression coefficients for all intensity measures and tectonic environments

Table 3: Logistic regression coefficients for CAV_5 and CAV_{STD} for all tectonic environments

Table 4: Comparison of models for the considered IMs

FIGURE CAPTIONS

Figure 1: Distribution of magnitude and distance in the dataset for the (a) shallow crustal, (b) intraplate, and (c) subduction tectonic environments

Figure 2: Distribution of site shear wave velocity for the (a) shallow crustal, (b) intraplate, and (c) subduction tectonic environments

Figure 3: Cumulative absolute velocity versus moment magnitude for the (a) shallow crustal, (b) intraplate, and (c) subduction tectonic environments

Figure 4: Cumulative absolute velocity versus distance to rupture for the (a) shallow crustal, (b) intraplate, and (c) subduction tectonic environments

Figure 5: Comparison of CAV attenuation in shallow crustal events with Campbell and Bozorgnia (2010) for selected earthquakes (a: Northridge, M_W 6.69; b: Loma Prieta, M_W 6.93; and c: Chi Chi, M_W 7.62)

Figure 6: Comparison of CAV attenuation in subduction events with Foulser-Piggott and Goda (2015) for selected earthquakes (a: Tohoku – 11 March 2011, interface, M_W 9.0; b: 12 June 2006, intraslab, 146km depth, M_W 6.2; 4 November 2002, interface, M_W 5.7)

Figure 7: CAV attenuation in intraplate events for selected earthquakes (a: Val-des-Bois, M_W 5.10; Au Sable Forks, M_W 4.99; Virginia, M_W 5.74)

Figure 8: Probabilities of nonzero CAV_5 for various event magnitudes in the (a) shallow crustal, (b) intraplate, and (c) subduction tectonic environments

Figure 9: Total residuals for CAV plotted against predictor variables for shallow crustal events

Table 1: Definitions of the considered intensity measures

IM	Definition	Reference
AI	$AI = \frac{\pi}{2g}\int_0^{t_d} a(t)^2 dt$	Arias (1970)
CAV	$CAV = \int_0^{t_d} \lvert a(t)\rvert dt$	EPRI (1988)
CAV_5	$CAV_5 = \int_0^{t_d} \langle\chi\rangle \lvert a(t)\rvert dt$	Kramer and Mitchell (2006)
CAV_{STD}	$CAV_{STD} = \sum_{i=1}^{N}\left(H(PGA_i - 0.025)\int_{i-1}^{i} \lvert a(t)\rvert dt\right)$	EPRI (2006)
V_{gi}	$V_{gi} = \max\left(\int_{t_1^i}^{t_2^i} \lvert a(t)\rvert dt\right)$	-

Table 2: Regression coefficients for all intensity measures and tectonic environments

	IM	a_0	a_1	a_2	b_1	b_2	b_3	b_4	f_1	f_2	τ	φ	σ_T
Shallow Crustal	AI	-18.784	7.758	-0.576	-4.013	0.435	-0.0213	-	0.005	-0.580	0.786	0.747	1.084
	CAV	-5.800	3.593	-0.231	-1.415	0.138	-0.0070	-	-0.155	-0.343	0.398	0.331	0.518
	CAV_5	-9.397	5.356	-0.395	-3.372	0.381	-0.0110	-	-0.197	-0.231	0.490	0.530	0.722
	CAV_{STD}	-10.836	5.165	-0.335	-1.563	0.087	-0.0019	-	-0.129	-0.273	0.529	0.392	0.658
	V_{gi}	-8.283	4.480	-0.353	-2.724	0.294	-0.0064	-	0.071	-0.390	0.545	0.452	0.708
Intraplate	AI	-33.761	11.016	-0.717	-0.421	-0.125	-0.0093	-	0	0	0.534	0.325	0.625
	CAV	-13.063	5.078	-0.273	0.439	-0.145	-0.0047	-	0	0	0.262	0.411	0.487
	CAV_5	-28.527	8.034	-0.157	2.913	-0.825	-0.0089	-	0	0	0.463	0.553	0.721
	V_{gi}	-3.029	0.931	0.040	-0.828	0.048	-0.0034	-	0	0	0.340	0.483	0.591
Subduction (Interface)	AI	-15.390	3.704	0.201	0.692	-0.774	0.0107	0	-	-	0.582	0.675	0.891
	CAV	-3.674	1.740	0.098	0.381	-0.334	0.0047	0	-	-	0.319	0.298	0.437
	CAV_5	-5.796	1.876	0.311	0.484	-0.699	0.0067	0	-	-	0.752	0.567	0.942
	CAV_{STD}	3.684	-0.575	0.335	0.565	-0.503	0.0071	0	-	-	0.406	0.222	0.463
	V_{gi}	-8.735	2.454	0.052	0.231	-0.354	0.0060	0	-	-	0.343	0.425	0.546
Subduction (Intraslab)	AI	-15.390	3.704	0.201	0	-0.615	0	0.0180	-	-	0.582	0.675	0.891
	CAV	-3.674	1.740	0.098	0	-0.250	0	0.0066	-	-	0.319	0.298	0.437
	CAV_5	-5.796	1.876	0.311	0	-0.572	0	0.0161	-	-	0.752	0.567	0.942
	CAV_{STD}	3.684	-0.575	0.335	0	-0.357	0	0.0089	-	-	0.406	0.222	0.463
	V_{gi}	-8.735	2.454	0.052	0	-0.289	0	0.0095	-	-	0.343	0.425	0.546
Subduction (Unknown)	AI	-15.969	4.203	0.092	-0.383	-0.538	0.0051	0.0195	-	-	0.659	0.683	0.949
	CAV	-4.865	2.108	0.036	-0.009	-0.220	0.0014	0.0074	-	-	0.312	0.302	0.434
	CAV_5	-0.902	2.471	0.131	-2.611	-0.289	0.0087	0.0268	-	-	0.876	0.869	1.234
	CAV_{STD}	-9.658	0.705	0.314	3.364	-0.702	-0.0035	0.0191	-	-	0.423	0.247	0.490
	Vgi	1.126	1.343	-0.062	-2.737	0.182	0.0013	0.0110	-	-	0.384	0.421	0.570

Table 3: Logistic regression coefficients for CAV_5 and CAV_{STD} for all tectonic environments

	IM	α_0	α_1	β_1	β_2	β_3
Shallow Crustal	CAV_5	-7.232	3.364	-1.775	-0.029	0
	CAV_{STD}	-5.780	3.194	-3.143	-0.011	0
Intraplate	CAV_5	-13.484	3.663	-0.223	-0.025	0
Subduction	CAV_5	0.4919	3.0830	-4.0998	-0.0044	0.0278
	CAV_{STD}	2.3897	3.3157	-5.9813	0.0060	0.0401

Table 4: Comparison of models for the considered IMs

	IM	Model	Ranges of Applicability		Number of Rock Records	Total Logarithmic Standard Deviation (σ_T)
Shallow Crustal	AI	This study	$4 \leq M_W \leq 8$	$0 \leq R \leq 200$	1,033	0.959
		Campbell and Bozorgnia 2010	$5 \leq M_W \leq 7.5$ - 8.5	$0 \leq R \leq 100$-200	150-200	0.831
		Travasarou et al. 2003	$4.7 \leq M_W \leq 7.6$	$0 \leq R \leq 400$	183	0.870
		Foulser-Piggott and Stafford 2011	$4 \leq M_W \leq 8$	$0 \leq R \leq 100$	150-200	1.127
		Danciu and Tselentis 2007	$4.5 \leq M_W \leq 7.0$	$0 \leq R \leq 150$	75	0.524
		Stafford et al. 2009	$5.1 \leq M_W \leq 7.5$	$0 \leq R \leq 300$	Unreported	1.145
	CAV	This study	$4 \leq M_W \leq 8$	$0 \leq R \leq 200$	1,033	0.521
		Campbell and Bozorgnia 2010	$5 \leq M_W \leq 7.5$ - 8.5	$0 \leq R \leq 100$-200	150-200	0.420
		Du and Wang 2013	$4.0 \leq M_W \leq 8.0$	$0 \leq R \leq 150$	197	0.416
		Danciu and Tselentis 2007	$4.5 \leq M_W \leq 7.0$	$0 \leq R \leq 150$	75	0.272
	CAV_5	This study	$4 \leq M_W \leq 8$	$0 \leq R \leq 200$	669	0.766
		Kramer and Mitchell 2006	$4.7 \leq M_W \leq 7.4$	$0 \leq R \leq 100$	282	0.707
		Danciu and Tselentis 2007	$4.5 \leq M_W \leq 7.0$	$0 \leq R \leq 150$	75	0.595
	CAV_{STD}	This study	$4 \leq M_W \leq 8$	$0 \leq R \leq 200$	383	0.658
		EPRI 2006	$4 \leq M_W \leq 8$	$0 \leq R \leq 200$	200-250	0.460
Subduction	AI	This study	$4 \leq M_W \leq 9$	$0 \leq R \leq 300$	1,237	0.891
		Foulser-Piggott and Goda 2015	$5 \leq M_W \leq 9$	$0 \leq R \leq 300$	Unreported	1.373
	CAV	This study	$4 \leq M_W \leq 9$	$0 \leq R \leq 300$	1,237	0.437
		Foulser-Piggott and Goda 2015	$5 \leq M_W \leq 9$	$0 \leq R \leq 300$	Unreported	0.642

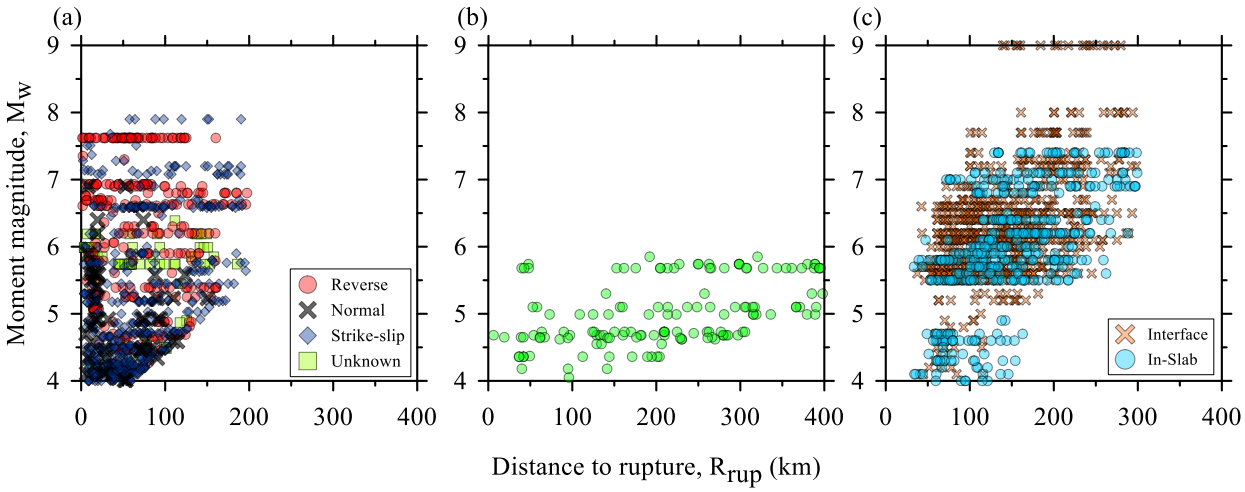

Figure 1: Distribution of magnitude and distance in the dataset for the (a) shallow crustal, (b) intraplate, and (c) subduction tectonic environments

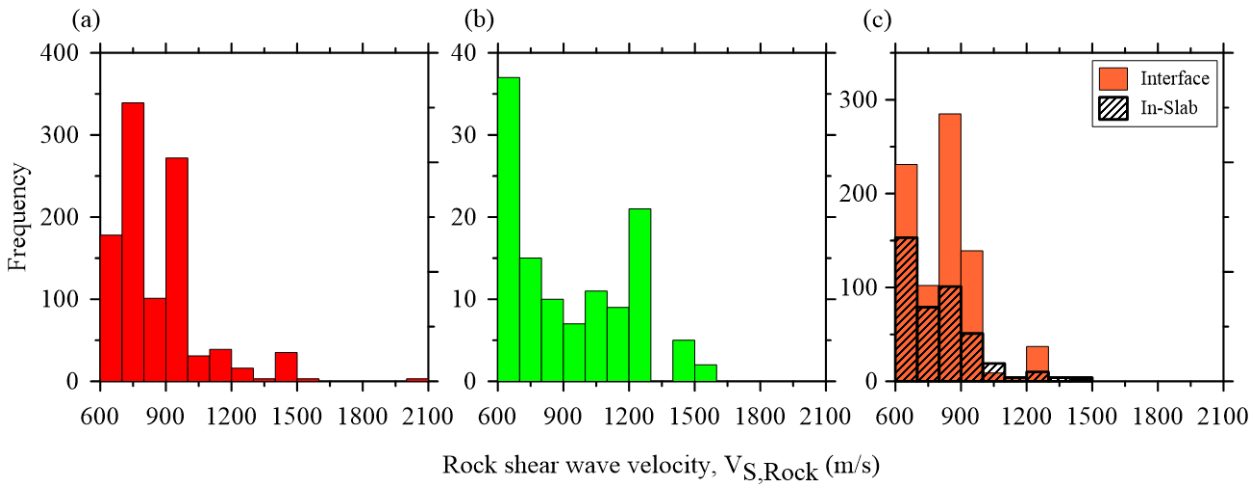

Figure 2: Distribution of site shear wave velocity for the (a) shallow crustal, (b) intraplate, and (c) subduction tectonic environments

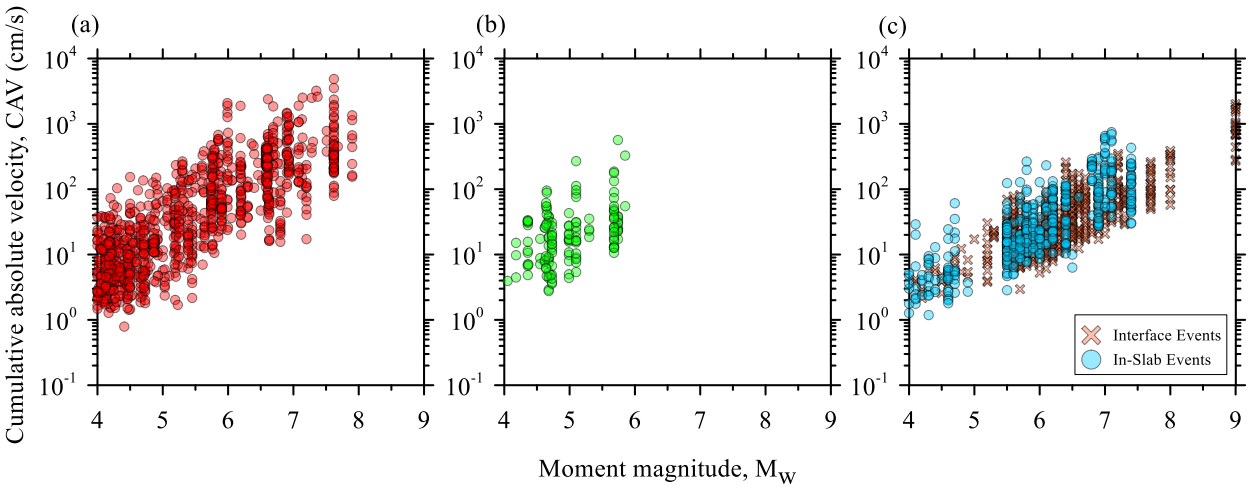

Figure 3: Cumulative absolute velocity versus moment magnitude for the (a) shallow crustal, (b) intraplate, and (c) subduction tectonic environments

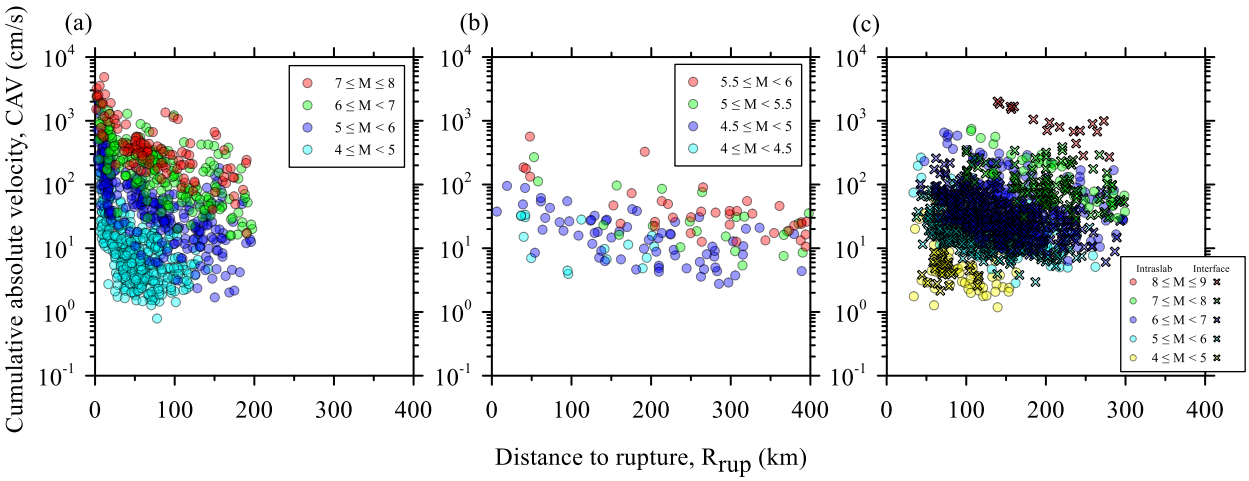

Figure 4: Cumulative absolute velocity versus distance to rupture for the (a) shallow crustal, (b) intraplate, and (c) subduction tectonic environments

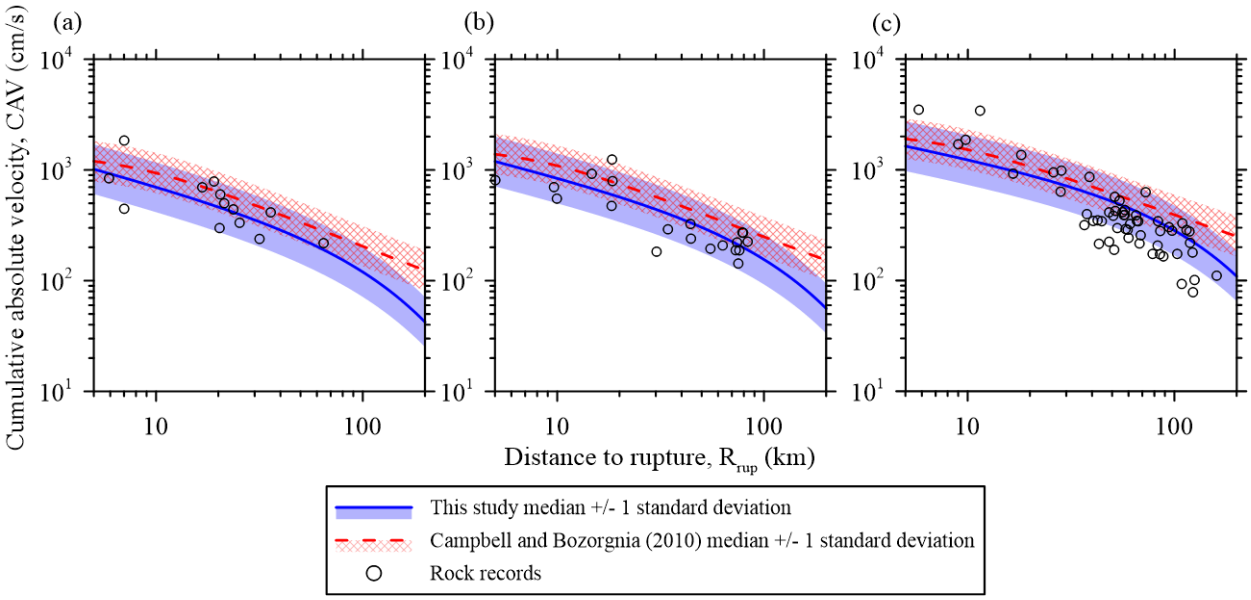

Figure 5: Comparison of CAV attenuation in shallow crustal events with Campbell and Bozorgnia (2010) for selected earthquakes (a: Northridge, M_W 6.69; b: Loma Prieta, M_W 6.93; and c: Chi Chi, M_W 7.62)

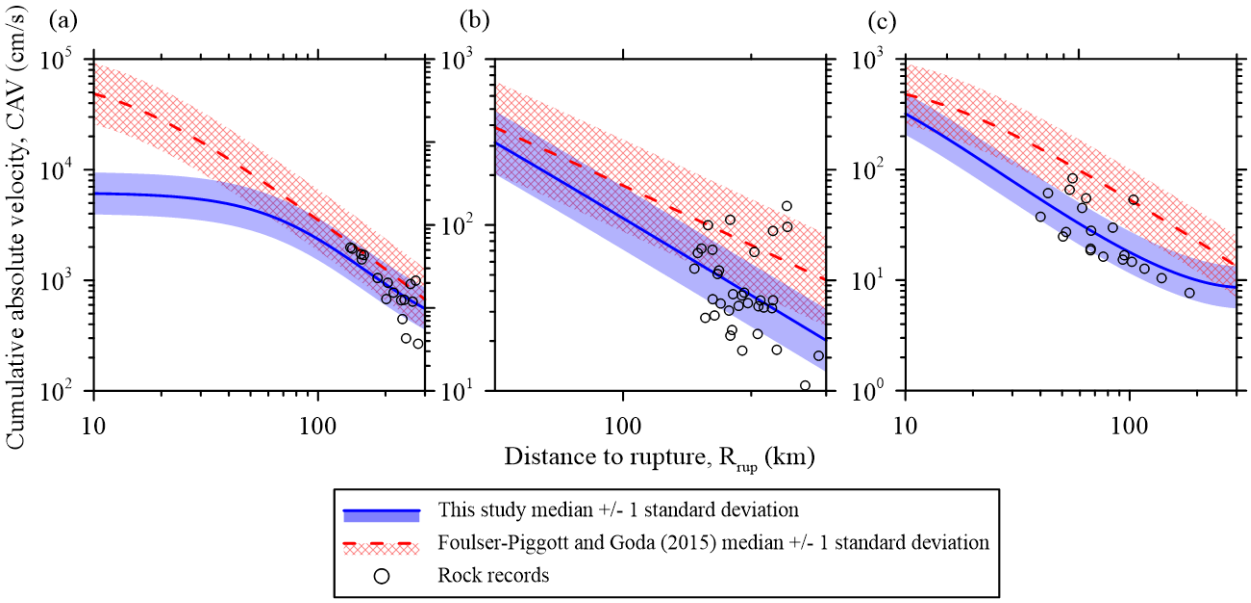

Figure 6: Comparison of CAV attenuation in subduction events with Foulser-Piggott and Goda (2015) for selected earthquakes (a: Tohoku – 11 March 2011, interface, M_W 9.0; b: 12 June 2006, intraslab, 146km depth, M_W 6.2; 4 November 2002, interface, M_W 5.7)

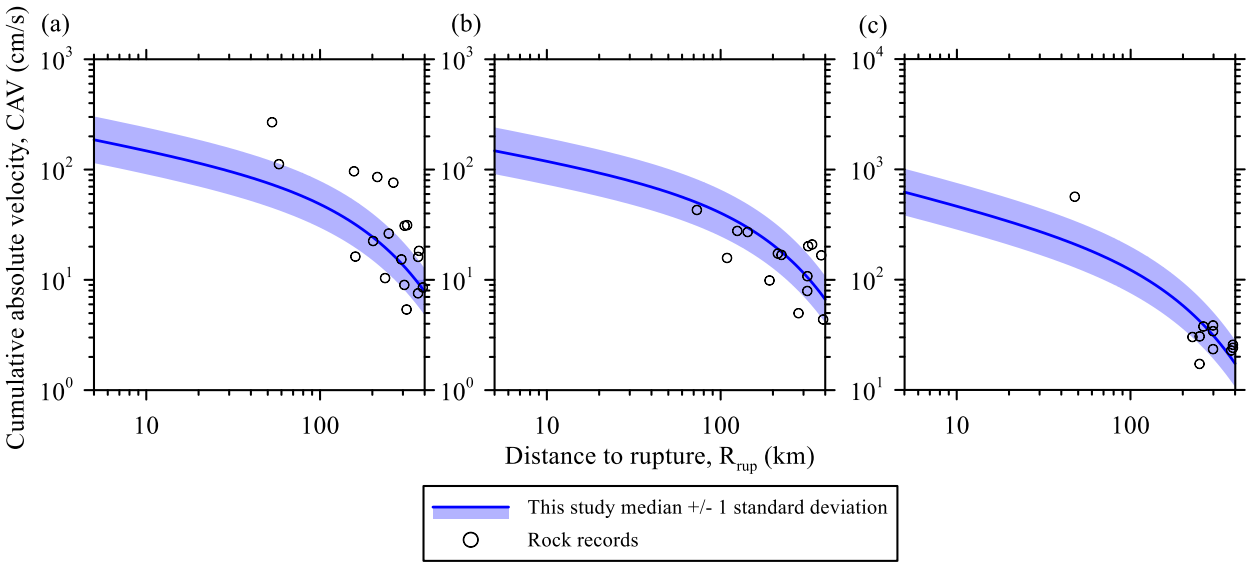

Figure 7: CAV attenuation in intraplate events for selected earthquakes (a: Val de Bois, M_W 5.10; Au Sable Forks, M_W 4.99; Virginia, M_W 5.74)

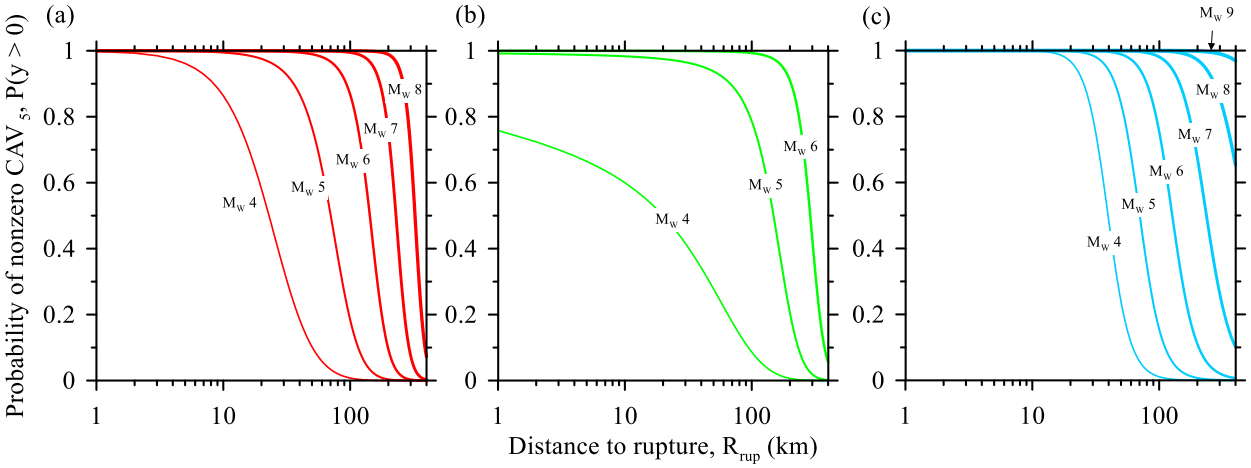

Figure 8: Probabilities of nonzero CAV_5 for various event magnitudes in the (a) shallow crustal, (b) intraplate, and (c) subduction tectonic environments

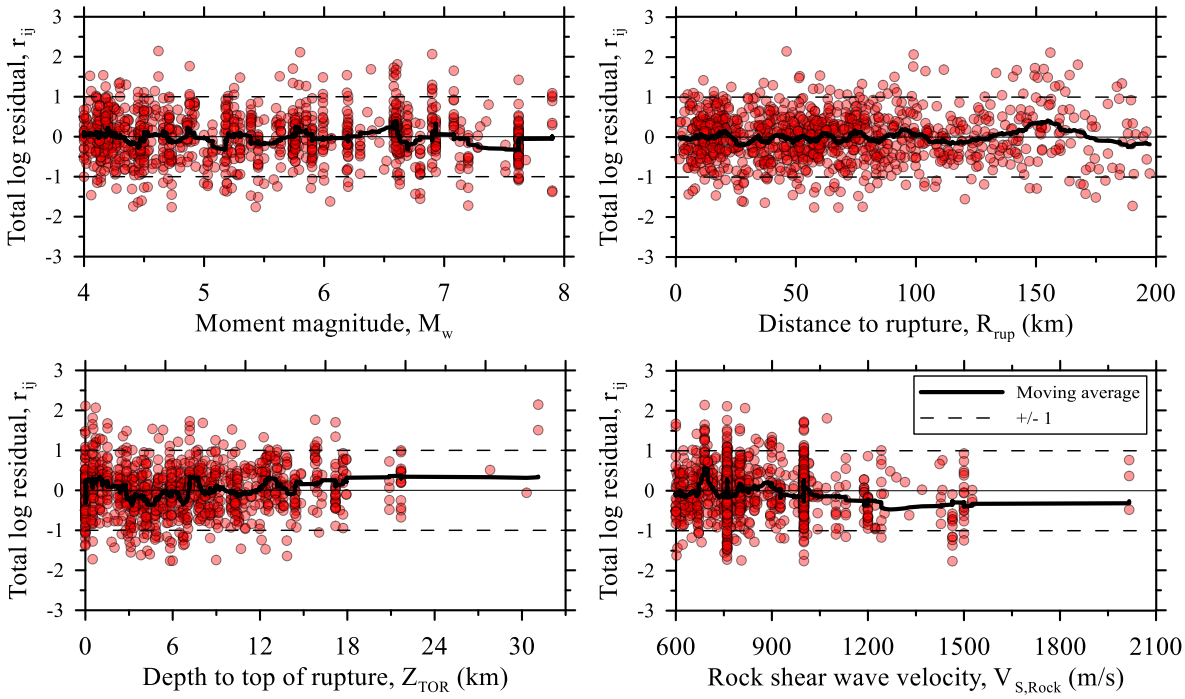

Figure 9: Total residuals for CAV plotted against predictor variables for shallow crustal events

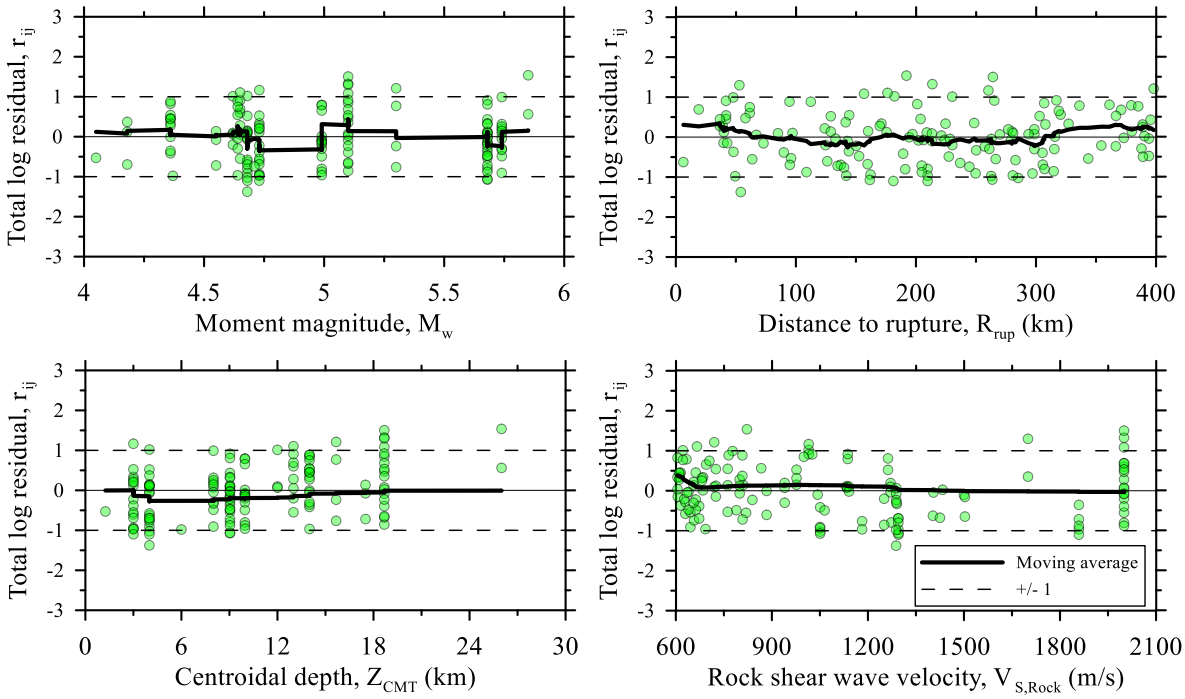

Figure 10: Total residuals for CAV plotted against predictor variables for intraplate events

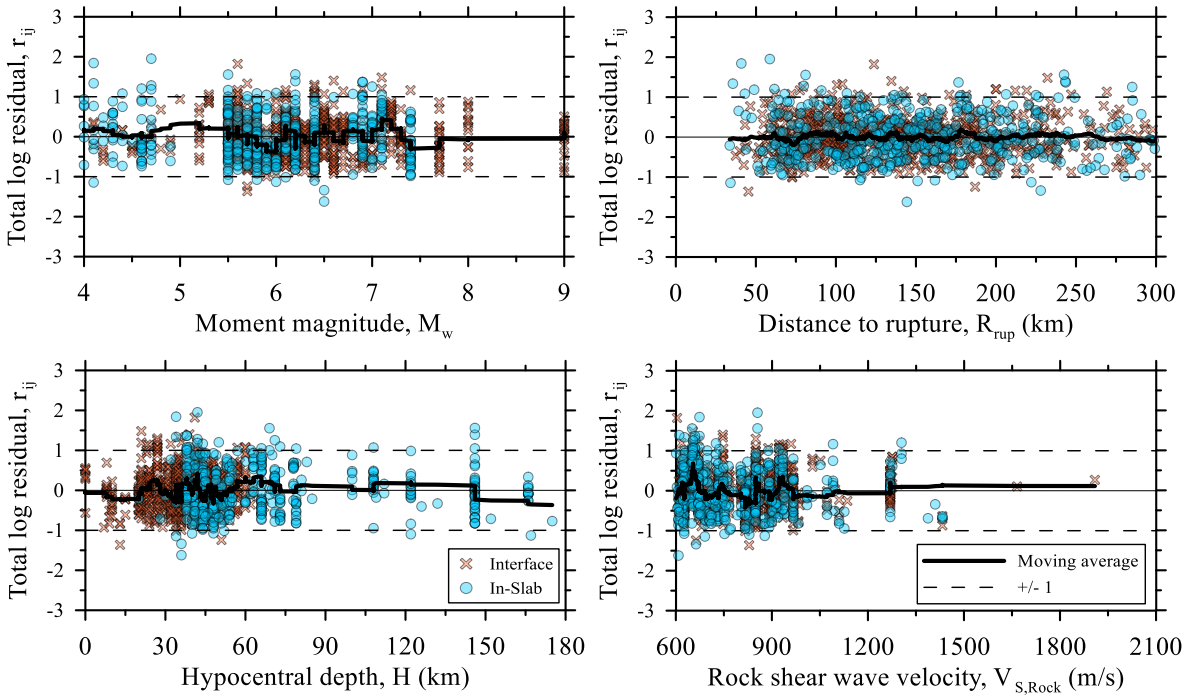

Figure 11: Total residuals for CAV plotted against predictor variables for subduction events

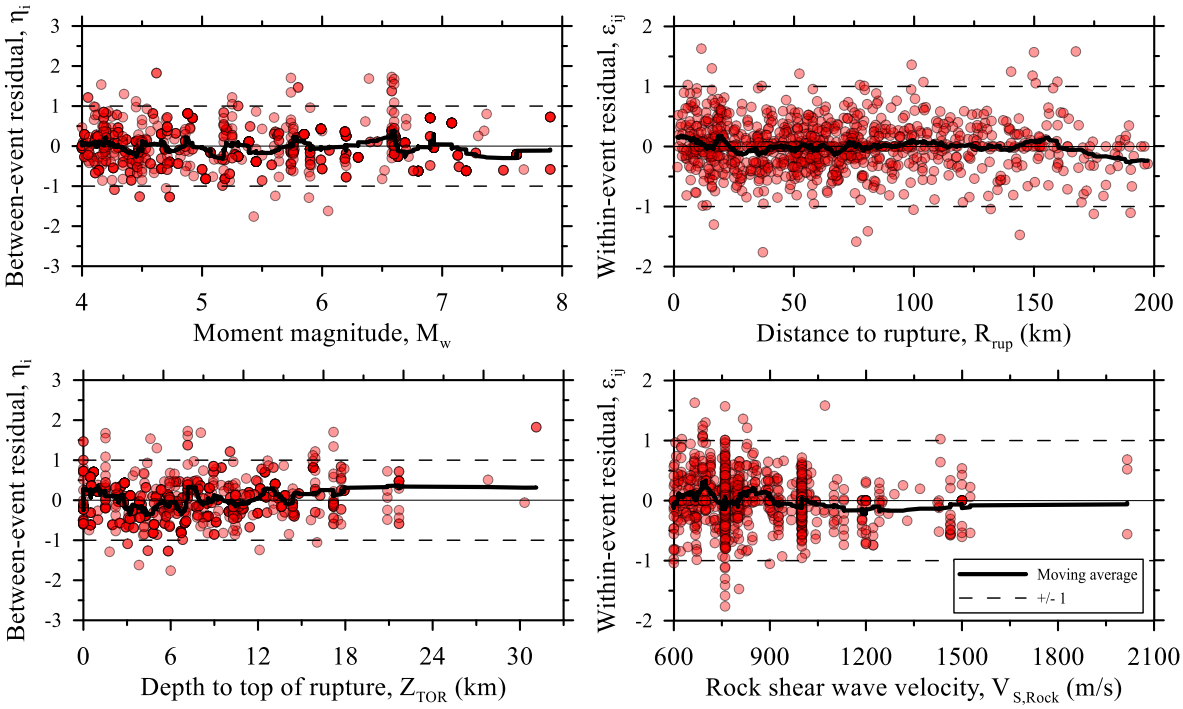

Figure 12: Between- and within-event residuals for CAV plotted against predictor variables for shallow crustal events

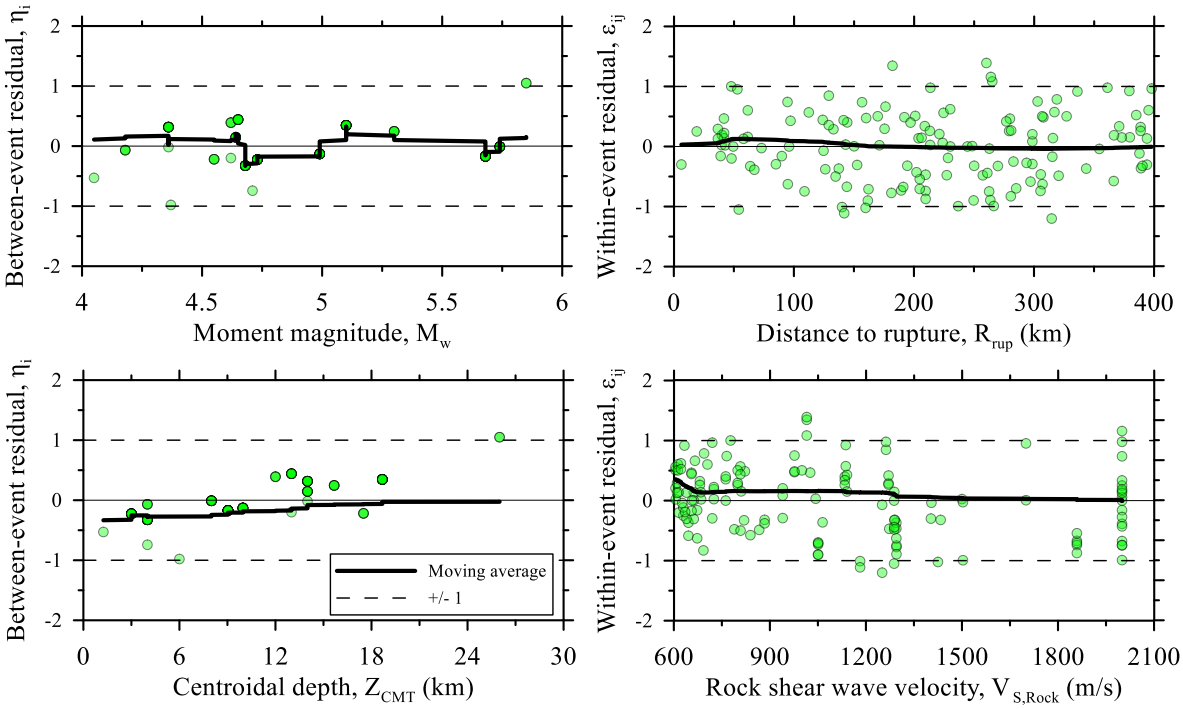

Figure 13: Between- and within-event residuals for CAV plotted against predictor variables for intraplate events

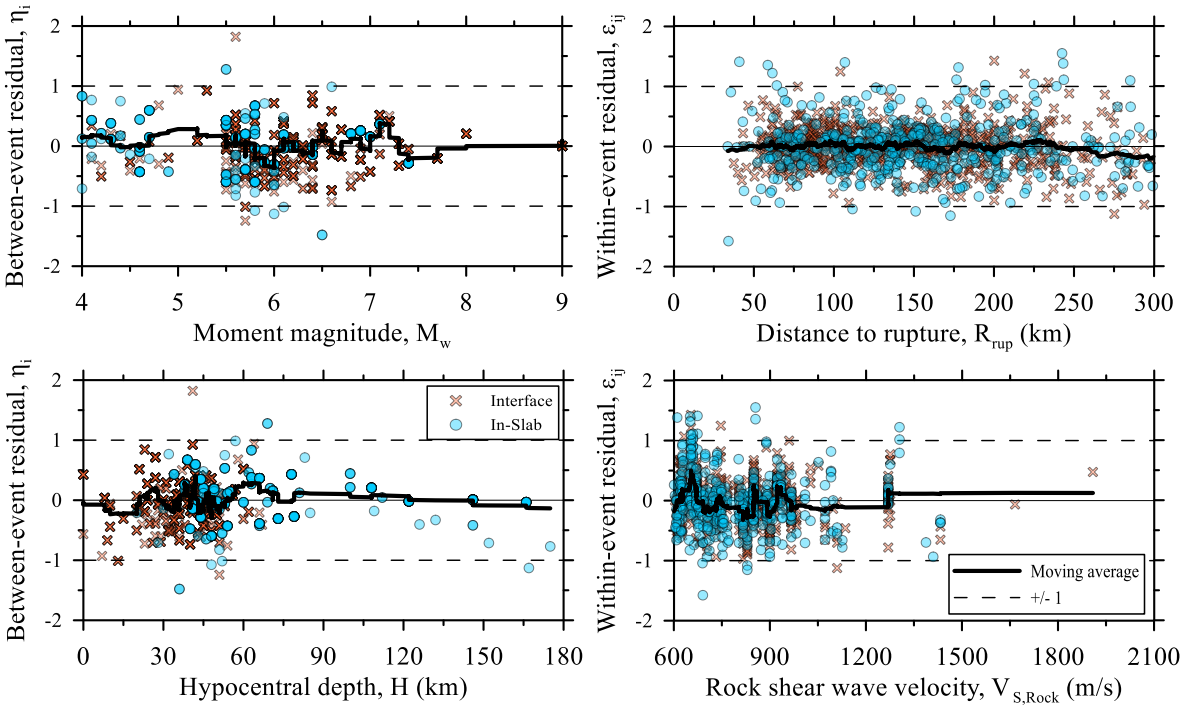

Figure 14: Between- and within-event residuals for CAV plotted against predictor variables for subduction events

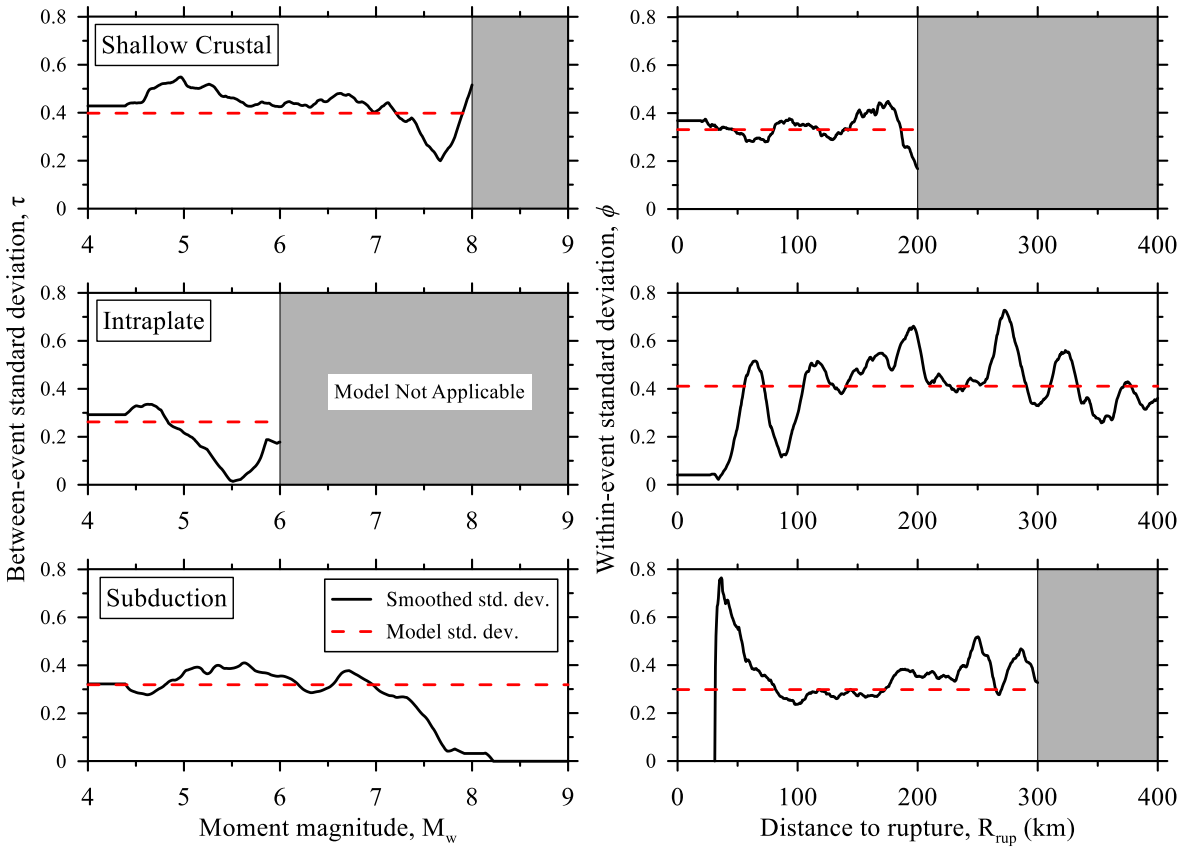

Figure 15: Smoothed and model between- and within-event standard deviations for CAV; the ranges of magnitude and distance for which the models are not applicable are shaded